Impact of high-density photocarrier generation on the conversion efficiency of a photodiode used as a laser power converter

Hanakuma, Ryota
Kan, Ichinori
Asahi, Shigeo
Harada, Yukihiro
Kita, Takashi

(Citation)
Japanese Journal of Applied Physics,64(7):074001

(Issue Date)
2025-07-01

(Resource Type)
journal article

(Version)
Version of Record

Japanese Journal of
Applied Physics

The Japan Society
of Applied Physics

Impact of high-density photocarrier generation on the conversion efficiency of a photodiode used as a laser power converter

OPEN ACCESS

Japanese Journal of Applied Physics **64**, 074001 (2025) **REGULAR PAPER**

https://doi.org/10.35848/1347-4065/ade414

Impact of high-density photocarrier generation on the conversion efficiency of a photodiode used as a laser power converter

Ryota Hanakuma, Ichinori Kan, Shigeo Asahi, Yukihiro Harada, and Takashi Kita*

Department of Electrical and Electronic Engineering, Graduate School of Engineering, Kobe University, 1-1 Rokkodai, Nada, Kobe 657-8501, Japan

*E-mail: kita@eedept.kobe-u.ac.jp

Received April 17, 2025; revised May 30, 2025; accepted June 11, 2025; published online June 30, 2025

We studied the photovoltaic properties of an InGaAs photodiode from the viewpoint of application as a laser power converter. The short-circuit current increased linearly with the excitation power density, but the open-circuit voltage was significantly influenced by carrier scattering when the excitation power density exceeded a critical excitation power density of 200 mW cm^{-2}. We found that the external luminescence efficiency, which is directly related to the open-circuit voltage, starts to decrease above 200 mW cm^{-2} due to an increase in the non-radiative recombination rate. This mechanism including its effect on the fill factor determines the value of the optimum excitation power density for this device.

Supplementary material for this article is available online

1. Introduction

Laser power transmission (LPT) is an emerging technology for wireless power transmission, and its main advantage is a high potential for power transmission over long distances due to the high directionality of laser light.[1–4] In LPT applications, a remote electronic device is powered through a laser power converter (LPC), which receives the incoming laser light. The power densities that need to be delivered depend on the device, and common applications may demand a few watts.[5] The most important task in the field of LPT is to develop methods to maximize the utilization efficiency of the supplied light energy.[6–10] The conversion efficiency strongly depends on the excitation power density. According to Fig. 4 (d) of Ref. 11, the maximum conversion efficiency of a conventional single junction silicon photodiode was 20.9% at 980 nm and an excitation power density of 5 mW cm^{-2}. At the same excitation conditions, the calculated conversion efficiency is 39.2%, which is a semiempirical value calculated using the measured EQE data. The theoretical efficiency limit increases with the excitation power density and becomes 41.5% at 25 mW cm^{-2}, but actual device efficiency measured at the same excitation power density has decreased to 13%, which is significantly below the ideal value due to Joule heating.[11]

The use of high excitation power densities is in principle favorable for photovoltaics because the splitting between the quasi-Fermi levels of the electrons and the holes becomes larger and also the photocurrent increases as the power density of the light irradiating the *p–n* junction of the considered photovoltaic device is increased. The simultaneous increase in both the output voltage and the current initially leads to a higher energy conversion efficiency under stronger illumination. However, high current densities can give rise to detrimental thermal effects due to Joule heating.[12–14] To avoid a performance limitation due to Joule heating, the relative contributions of voltage and current to the electrical power need to be adjusted, for example by using appropriate wide-bandgap semiconductors or multi-junction structures.[15–19] Such improvements are also necessary for LPCs. Efficient energy conversion is particularly important for LPCs exposed to high excitation-power densities, where thermal effects are stronger and thus can seriously affect the photovoltaic properties determining the conversion efficiency. Note that the photovoltaic conversion efficiency tends to decrease almost linearly as the device temperature (T_c) increases.[14,20]

In our previous work, we studied the photovoltaic properties of a conventional silicon photodiode under monochromatic illumination conditions to clarify the loss mechanisms related to LPT.[11] We found that the photovoltaic output is influenced by Joule heating if the excitation power density exceeds a certain critical level, and that this leads to an excitation-power density dependence of the optimum excitation wavelength. Since silicon is an indirect bandgap semiconductor, all optical responses in the measured device were assisted by phonons. In this work, we studied the photovoltaic properties of an InGaAs photodiode to elucidate the loss mechanisms related to LPT in the case of a direct-bandgap semiconductor, which provides more efficient optical responses.

2. Experimental methods

2.1. Optical power receiver

We employed an InGaAs photodiode designed to measure the output power of pulsed and continuous-wave laser sources (Thorlabs SM05PD5A). The detection area of this device is 3.1 mm^2, the device is covered by a quartz glass, and operation up to at least 85 °C should be possible. This device has an anti-reflective coating.

2.2. External-quantum-efficiency measurements

The measurement of the external quantum efficiency (EQE) was performed at room temperature (298 K) without a temperature controller. The device was illuminated with monochromatic light with a full width at half-maximum of 4 nm, which was obtained using the white light generated by a tungsten-halogen lamp and a 140 mm single monochromator (Horiba Micro HR). The excitation beam was modulated at 407 Hz by an optical chopper and the spot diameter on the photodiode was approximately 2 mm. The excitation wavelength was scanned from 1300 to 1700 nm, and the output current under the short-circuit condition was amplified by a current amplifier (Femto DHPCA-100) and then detected by a lock-in amplifier (Ametek Signal Recovery 5210) synchronized with the chopper. The intensity of the used monochromatic beam varied between 17–52 μW cm^{-2}, and the integrated power density of the tungsten-halogen lamp in the wavelength range 1300–1700 nm was approximately 1.4 mW cm^{-2}. The incident light intensity was measured directly above the InGaAs photodiode device using an optical power sensor (Coherent OP-2 IR). Note that we used an optical fiber to deliver the light to the device.

2.3. Current–voltage measurements

The photovoltaic properties for laser power conversion were characterized by measuring the current-density–voltage (*J–V*) curve and the electrical output power at the maximum power point for different excitation densities. Here, we used a 1550 nm continuous-wave solid-state laser as a light source. At this wavelength, the photodiode has a nominal responsivity of about 1 A/W for a load of 50 Ω. The diameter of the beam spot on the device was 0.82 mm, and the generated photocurrent was detected as a function of the applied bias voltage using a source measure unit (Keithley SourceMeter 2400). These measurements were conducted without active cooling.

2.4. Determination of the device temperature

In order to be able to account for the excitation power dependence of the device temperature in our analysis, we analyzed the actual changes in the bandgap energy. Because the temperature of the device increased with the excitation power density, we were able to confirm a shift in the bandgap energy. We measured the EQE spectrum near the bandgap under 1550 nm excitation and assumed that the observed temperature dependence of the bandgap obeys the well-known Varshni function.[21,22] The temperature increase caused by the additional monochromatic beam for the EQE measurement should be negligible due to the extremely weak excitation power density of less than 52 μW cm^{-2}.

3. Results and discussion

The EQE spectrum of the InGaAs photodiode at room temperature is shown in Fig. 1. The absorption edge appears around 1650 nm. Since the excitation wavelength for the laser-power-conversion experiment (1550 nm) is close to this value, the excess energy of the generated carriers is small. Figure 2 summarizes the results of the laser-power-conversion experiment: the short-circuit current density (J_{SC}), the open-circuit voltage (V_{OC}), the fill factor (FF), the conversion efficiency (η) at the maximum power point, the device temperature (T_c), and the external luminescence efficiency (f_c) are plotted as a function of the excitation power density. The device temperature is required to determine f_c. Note that f_c (which lies within the range $0 \leqslant f_c \leqslant 1$)[23,24] can be defined using the following equation:[24,25]

$$V_{OC} = V_{iOC} + V_c \ln f_c. \tag{1}$$

Here, V_{iOC} is the ideal (intrinsic) open-circuit voltage and $V_c = k_B T_c/e$, where k_B is the Boltzmann constant and e is the elementary charge. The value of V_{iOC} can be determined using $V_{iOC} = V_c \ln(F_s/F_{c0} + 1)$,[23] where F_s and F_{c0} are the

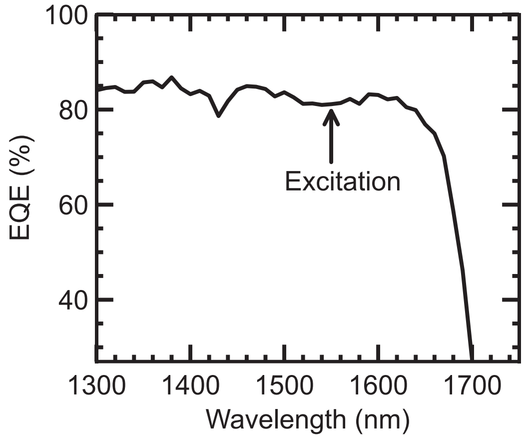

Fig. 1. The EQE spectrum of the InGaAs photodiode. A small OH absorption peak appears around 1400 nm since we used an optical fiber, and the excitation wavelength for the laser-power-conversion experiment is indicated by the arrow.

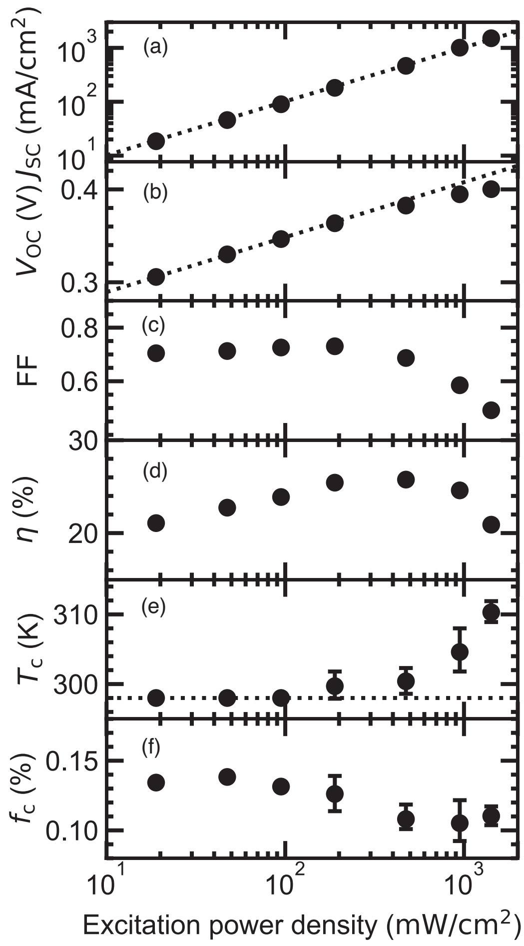

Fig. 2. The excitation-power density dependence of (a) J_{SC}, (b) V_{OC}, (c) FF, (d) η, (e) T_c, and (f) f_c. These parameters were measured using an excitation wavelength of 1550 nm.

electron–hole pair generation rates due to optical excitation and the thermal activation, respectively. Since the sign of the second term on the right-hand side of Eq. (1) is negative, V_{OC} is smaller than the ideal value, and the difference between V_{iOC} and V_{OC} becomes larger as the contribution of non-radiative recombination increases.

Figure 2(a) clarifies that J_{SC} increases linearly with the excitation power density (the dotted line indicates the

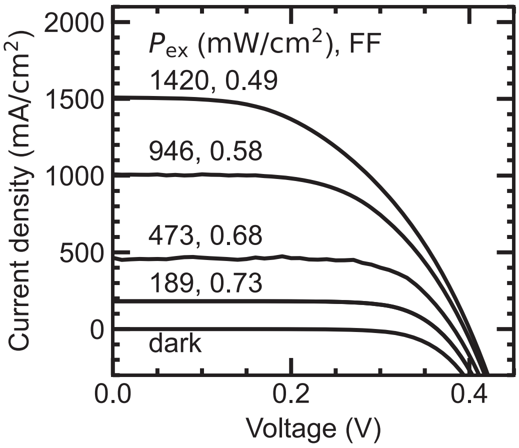

Fig. 3. *J–V* curves obtained using different excitation conditions.

dependence predicted from the EQE). On the other hand, the data for V_{OC} in Fig. 2(b) starts to deviate from the initially observed linear relationship in this semi-log plot when the excitation power density exceeds 200 mW cm^{-2} (the dotted line indicates a semiempirical linear line utilizing the average f_c value measured below the critical excitation power density). We observed a similar change for a conventional silicon photodiode (with a nominal responsivity of 0.5 A W^{-1} at 960 nm),[11] but the critical excitation power density was about 2 mW cm^{-2}, which is almost two orders of magnitude smaller than the value observed in Fig. 2(b). To confirm the loss mechanism in the InGaAs photodiode, we consider the behavior of the FF, η, T_c, and f_c data in Figs. 2(c)–2(f), which also show characteristic changes near 200 mW cm^{-2}. The observed f_c of Si is one to two orders of magnitude smaller than that of InGaAs, which is direct evidence demonstrating the contribution of the phonon-assisted light absorption process in indirect bandgap Si.

The dotted line in Fig. 2(e) indicates that the temperature of the photodiode without excitation is 298 K. Since the temperature of the photodiode was not actively controlled, T_c should increase with the excitation power density. Figure 2(e) confirms that T_c starts to increase for excitation power densities above 200 mW cm^{-2}, and thus the data obtained using excitation power densities above this value are influenced by Joule heating. The conversion efficiency η in Fig. 2(d) first increases with the excitation power density, because both J_{SC} and V_{OC} increase. However, due to the abrupt change in the FF near 200 mW cm^{-2} [Fig. 2(c)], η reaches its maximum at around 200–450 mW cm^{-2}. Before thermal effects appear, i.e., below the critical excitation power density, the conversion efficiency is mainly determined by transmission loss and thermal loss. Here, thermal loss arises from excess photon energy above the bandgap, and transmission loss depends on the absorption coefficient. Hence, the photon energy of the excitation light against the bandgap has a strong impact on conversion efficiency as shown in Fig. 3 of Ref. 11. The relatively small efficiency observed for Si rather than that of InGaAs is dominantly caused by the relatively large transmission loss (small absorption coefficient) near the fundamental bandgap of the indirect bandgap Si. On the other hand, the critical excitation power density, at which the influence of Joule heating starts to appear, is determined by the contribution of

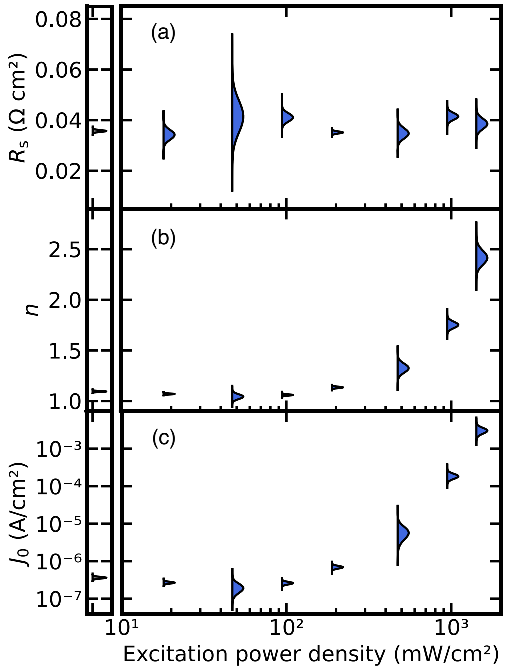

Fig. 4. The excitation-power density dependence of the estimated distributions of (a) R_s, (b) n, and (c) J_0. The results obtained in the dark are shown in a separate panel on the left-hand side.

phonon-assisted non-radiative processes and strongly depends on f_c. Figure 3 shows the *J–V* curves obtained using different excitation conditions. The shape of the *J–V* curve depends strongly on the excitation power density P_{ex}: it deviates stronger from the ideal shape (with an FF close to unity) as the excitation power density increases. An increase in the excess carrier density increases the impact of Joule heating, and hence T_c rises.

To clarify the details, we determined the diode quality factor (n), the series resistance (R_s), and the dark saturation current density (J_0) as a function of the excitation power density using a single-diode model:

$$J = J_{ph} - J_0\left\{\exp\left[\frac{q(V + JR_s)}{nk_B T_c}\right] - 1\right\} - \frac{V + JR_s}{R_{sh}}, \quad (2)$$

where J_{ph} is the photocurrent density and R_{sh} is the shunt resistance. We used the probabilistic programming framework Turing.jl for the Julia programming language[26] to estimate the equivalent-circuit parameters via Bayesian inference.[27] The diode quality factor indicates how close the actual diode characteristics are to those of an ideal diode, where the current is determined by carrier diffusion. A value of n close to 1 means that the diffusion current is dominant, and if it is close to 2, the generation–recombination current is dominant. In a *p–n* junction, the generation–recombination current is in general dominant at low forward-bias voltages, and the diffusion current becomes dominant as the forward-bias voltage is increased.

As shown in Fig. 4(a), R_s is almost independent of the excitation power density. This is consistent with the result of Ref. 28 where the change in R_s of the investigated $In_{0.3}Ga_{0.7}As$ cell around room temperature was small. On the other hand, the parameters n and J_0 in Figs. 4(b) and 4(c), respectively, exhibit a characteristic onset near

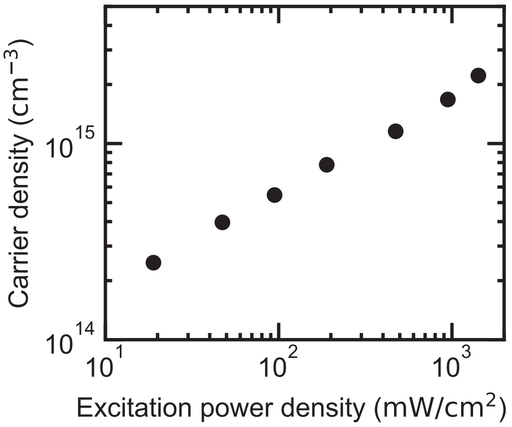

Fig. 5. The excitation-power density dependence of the carrier density under open-circuit conditions.

200 mW cm^{-2} like the data in Fig. 2. At low excitation power densities, n is close to 1, and for excitation power densities above 200 mW cm^{-2}, it increases. A region limited by the generation–recombination current was not observed, and the increase is attributed to Ohm's law with a nearly constant series resistance. To explain the behavior of J_0, we additionally consider the excess carrier density. The carrier density under open-circuit conditions can be estimated from the known values of V_{OC} and T_c and the intrinsic carrier density n_i:[29]

$$n = n_i \exp\left(\frac{qV_{OC}}{2k_B T_c}\right). \quad (3)$$

The excitation-power density dependence of the carrier density under the open-circuit condition estimated using Eq. (3) is shown in Fig. 5. At about 200 mW cm^{-2}, the carrier density exceeds 10^{15} cm^{-3} at which the mean carrier distance is approximately 100 nm. Such carrier distance at about 200 mW cm^{-2} is longer than that causing carrier-carrier scattering producing hot carriers. A higher non-radiative recombination rate is most likely caused by a higher inelastic electron–phonon scattering rate,[30] which agrees well with the excitation-power density dependence of f_c in Fig. 2(f). This means that non-radiative recombination processes become remarkable above 200 mW cm^{-2}. Furthermore, J_0 is inversely proportional to the square root of the carrier lifetime. The increase in J_0 due to the temperature increase shown in Fig. 2(e) (~10 K) is estimated to be less than one order of magnitude according to Ref. 28 while the actually observed increase is four orders of magnitude. Therefore, Fig. 4(c) indicates that the carrier lifetime is significantly reduced at high excitation power densities.

4. Conclusions

We studied the excitation power dependence of the J–V characteristics of an InGaAs photodiode used as an LPC. While the J_{SC} data showed a linear dependence on the excitation power density, there were obvious changes in the trends of the V_{OC} and FF data above 200 mW cm^{-2}. We have considered the fact that the open-circuit voltage is a function of the external luminescence efficiency, which in turn depends on the non-radiative recombination rate. The enhanced inelastic electron–phonon scattering rate and resulting Joule heating caused by the high excess carrier densities at higher excitation power densities led to a reduction in the conversion efficiency, and we observed a series-resistance effect in the J–V characteristics.

Acknowledgments

This work was partially supported by a Grant-in-Aid for Scientific Research (B) from the Japan Society for the Promotion of Science (JSPS) (KAKENHI Grant No. 23H01448) and the Advanced Technologies for Carbon-Neutral (ALCA-Next) program of the Japan Science and Technology Agency (JST) under Grant No. JPMJAN24B1. The authors thank Prof. Masaaki Nakayama at Osaka Metropolitan University for the valuable discussions on carrier scattering.

ORCID iDs

Shigeo Asahi https://orcid.org/0000-0003-1512-106X
Yukihiro Harada https://orcid.org/0000-0003-4784-6751

1) K. Jin and W. Zhou, IEEE Trans. Power Electron. **34**, 3842 (2019).
2) R. Jomen, F. Tanaka, T. Akiba, M. Ikeda, K. Kiryu, M. Matsushita, H. Maenaka, P. Dai, S. Lu, and S. Uchida, Jpn. J. Appl. Phys. **57**, 08RD12 (2018).
3) Y. Tai and T. Miyamoto, Energies **15**, 7388 (2022).
4) C. Algora, I. García, M. Delgado, R. Peña, C. Vázquez, M. Hinojosa, and I. Rey-Stolle, Joule **6**, 340 (2022).
5) S. Fafard and D. P. Masson, J. Appl. Phys. **130**, 160901 (2021).
6) J. Schubert, E. Oliva, F. Dimroth, W. Guter, R. Loeckenhoff, and A. W. Bett, IEEE Trans. Electron Devices **56**, 170 (2009).
7) D. Masson, F. Proulx, and S. Fafard, Prog. Photovoltaics Res. Appl. **23**, 1687 (2015).
8) H. Helmers, E. Lopez, O. Höhn, D. Lackner, J. Schön, M. Schauerte, M. Schachtner, F. Dimroth, and A. W. Bett, Phy. Status Solidi RRL **15**, 2100113 (2021).
9) Y. Wang, Z. Zheng, J. Wang, P. Bi, Z. Chen, J. Ren, C. An, S. Zhang, and J. Hou, Nat. Commun. **14**, 5511 (2023).
10) S. D. Jarvis, J. Mukherjee, M. Perren, and S. J. Sweeney, IET Optoelectron **8**, 64 (2014).
11) R. Hanakuma, S. Asahi, Y. Harada, and T. Kita, Jpn. J. Appl. Phys. **64**, 014001 (2025).
12) T. He, S.-H. Yang, H.-Y. Zhang, C.-M. Zhao, Y.-C. Zhang, P. Xu, and M. Á. Muñoz, Chin. Phys. Lett. **31**, 104203 (2014).
13) E. Oliva, F. Dimroth, and A. W. Bett, Prog. Photovolt: Res. Appl. **16**, 289 (2008).
14) J. Zhang et al., Mater. Res. Express **12**, 025902 (2025).
15) A.-C. Wang, Y.-R. Sun, S.-Z. Yu, J.-J. Yin, W. Zhang, J.-S. Wang, Q.-X. Fu, Y.-H. Han, J. Qin, and J.-R. Dong, Appl. Phys. Lett. **119**, 243902 (2021).
16) C. Guan, L. Li, H.-M. Ji, S. Luo, P. Xu, Q. Gao, H. Lv, and W. Liu, IEEE J. Photovolt. **8**, 1355 (2018).
17) E. Lopez, O. Höhn, M. Schauerte, D. Lackner, M. Schachtner, S. K. Reichmuth, and H. Helmers, Prog. Photovolt: Res. Appl. **29**, 461 (2021).
18) S. Fafard, M. C. A. York, F. Proulx, C. E. Valdivia, M. M. Wilkins, R. Arès, V. Aimez, K. Hinzer, and D. P. Masson, Appl. Phys. Lett. **108**, 071101 (2016).
19) P. Sanmartín, F. Almonacid, A. García-Loureiro, and E. F. Fernández, Proc. SPIE **13359**, 133590K (2025).
20) S. Chander, A. Purohit, A. Sharma, S. P. Nehra, and M. S. Dhaka, Energy Reports **1**, 175 (2015).
21) B. L. Anderson and R. L. Anderson, *Fundamentals of Semiconductor Devices* (McGraw-Hill, New York, 2017) 2nd ed.
22) D. K. Gaskill, N. Bottka, L. Aina, and M. Mattingly, Appl. Phys. Lett. **56**, 1269 (1990).

23) T. Kita, Y. Harada, and S. Asahi, *Energy Conversion Efficiency of Solar Cells* (Springer, Berlin, 2019).
24) O. D. Miller, E. Yablonovitch, and S. R. Kurtz, IEEE J. Photovolt. **2**, 303 (2012).
25) U. Rau, Phys. Rev. B **76**, 085303 (2007).
26) H. Ge, K. Xu, and Z. Ghahramani, Proc. of the Twenty-First Int. Conf. on Artificial Intelligence and Statistics, 1682 2018.
27) K. Tada, Appl. Phys. Express **14**, 046502 (2021).
28) G. Li, C. Wang, J. Lu, and H. Zhang, AIP Adv. **9**, 095053 (2019).
29) L. J. A. Koster, V. D. Mihailetchi, R. Ramaker, and P. W. M. Blom, Appl. Phys. Lett. **86**, 123509 (2005).
30) Z. Mics, A. D'Angio, S. A. Jensen, M. Bonn, and D. Turchinovich, Appl. Phys. Lett. **102**, 231120 (2013).